Large Eddy Simulation of lithium-ion vent gas explosions: effect of wall heat loss on tulip flame formation and propagation

A. Cellier*[1], F. Duchaine[1], T. Poinsot[2,1], G. Okyay[3], M. Leyko[3], and M. Pallud[4]

[1]CERFACS, 42 avenue Gaspard Coriolis, 31057 Toulouse, France
[2]Institut de Mécanique des Fluides de Toulouse, IMFT, Université de Toulouse, CNRS, Toulouse, France
[3]SAFT Batteries, 111 Boulevard Alfred Daney, 33074 Bordeaux, France
[4]TotalEnergies – OneTech, 92400 Courbevoie, France

Abstract

Large scale Lithium-ion batteries play a crucial role in the transition to green energy. However, when misused, such batteries may experience thermal runaway, characterized by the production of hot and flammable gases that eventually vent out. If ignition conditions are not met and the battery is confined, gases accumulate making the event of explosion probable. To assert the problem of creating reliable large scale storage systems, numerical simulations of Li-ion related explosions could be an efficient predicting tool at a prototyping step. Here, the focus is on the effect of wall heat losses on the tulip flame formation and propagation. It sets a first academic laminar case before considering Li-ion-related turbulent explosions, the long-term aim being high-fidelity simulations of industrial-size battery explosion scenarios.

Keywords: Lithium-ion battery vent gases, explosion scenario, large eddy simulation, tulip flame.

Introduction

In the event of a Thermal Runaway (TR) occurring in an enclosed space, if a fire is not immediately triggered, gases may accumulate until the lower flammability limit of the mixture is reached. A spark from a failing electrical device can trigger an explosion. At the scale of the cell, the explosion is already critical in some cases where the user is close to the system [1, 2], or when considering transportation applications [3]. In large scale batteries or in storage configurations, and due to TR propagation [4, 5], large quantity of gases can be released, filling the enclosed space, leading to dramatic explosions. Baird *et al.* [1] and Henriksen *et al.* [6] have listed accidents involving batteries, where an explosion occured. The storage and transportation of batteries also raise concerns at the highest levels [7], and predicting the explosion behavior of a given configuration involving failing Li-ion is critical. On the way to predict the explosion behavior of failing Li-ion batteries in confined spaces (storage, large scale power modules, ...), multiple interrogations can be highlighted concerning the capability of a solver to accurately reproduce all the phenomena involved. As an attempt to reproduce a Li-ion vent-gases-related explosion, the simulation of flames obtained experimentally by Henriksen *et al.* [6] where extensive data are available is proposed. In the following sections, the validation of the simulation framework against experimental data is given. Influences of boundary conditions are asserted on the way to this validation. Overall, this study sets a milestone towards the simulation of more complex explosions of Li-ion vent gases, with a familiarization to the phenomena at hand in a simple academic case, already used for experimental *versus* simulation comparisons [6].

1 Source of the experimental data

The experimental dataset is shared by Henriksen and Bjerketvedt [6]. A description of the experimental setup used to produce the data is recalled here: The tube is of rectangular cross-section (length 1000 mm, width 65 mm, height 116.5 mm), closed at the ignition end and opened at the venting end. The tube is filled at atmospheric conditions ($T_0 = 293.0\,\mathrm{K}, P_0 = 1.0$ atm) with a mixture of synthetic vent gases and air with predefined equivalence ratio. A 20 ms ignition sequence, consisting in two successive sparks, is triggered after a 1.0 min resting time. The system is equipped with four pressure sensors (Kistler 7001) and the high speed camera (Photron SA1) captures flame displacement through the optical access. A schematic description of the experimental setup is given in Figure 1. The gaseous mixture considered in the study of Henriksen *et al.* results from vent gas analysis of commercial LFP cells. The molar composition is as follows: H_2: 34.9 %, CH_4: 15.0 %, C_2H_4: 5.0 %, CO: 25.0 %, CO_2: 20.1 %.

2 Simulation framework and models

The approach to simulate the free flame proposed in this section serves two main objectives: 1. it is a direct opportunity to validate choices in terms of chemical kinetics modelling and flame modelling, 2. it is a first calibration step to go further with cases including obstacles producing turbulence and realistic battery modules. For the first objective, an Analytically Reduced Chemistry scheme (ARC) is chosen. It is developed and validated for multiple Li-ion vent gases under var-

*Corresponding author: cellier@cerfacs.fr

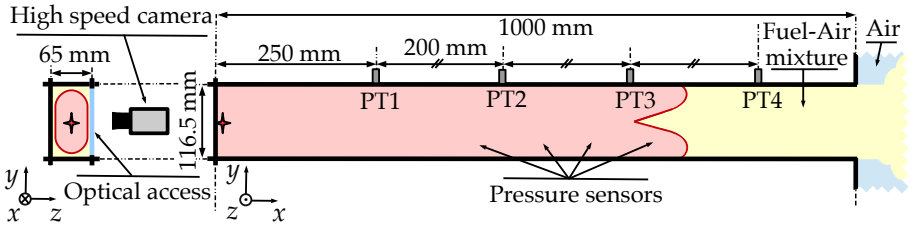

Figure 1: Schematic represesentation of the experimental setup proposed by Henriksen *et al.* [6] to assert Li-ion vent gases explosions. The four pressure transducers are noted PT1-4.

ious representative combustion scenario [8]. Figure 2 shows the good agreement between the reference detailed San Diego scheme (SD) and the reduced scheme (ARC) when computing a 1D premixed laminar flame at $T = 300\,\mathrm{K}$ and $P = 1$ atm. Concerning the flame model, the Dynamically Thickened Flame (DTF) approach is chosen [9, 10]. It ensures five points in the flame front thickness by detecting methane consumption and artificially thickening the flame. 46.3 M unstructured tetrahedra compose the mesh with a target resolution in the tube of 1.0 mm. This choice made in a case where a structured mesh would also perform properly is motivated by the fact that in cases where obstacles of arbitrary shapes are placed in the channel, this mesh topology will be mandatory. The calibration in this step concerns the way heat transfers at the wall are treated, which can be transposed further in turbulent cases, to assert the initial laminar propagation, important to avoid errors propagating through history effects.

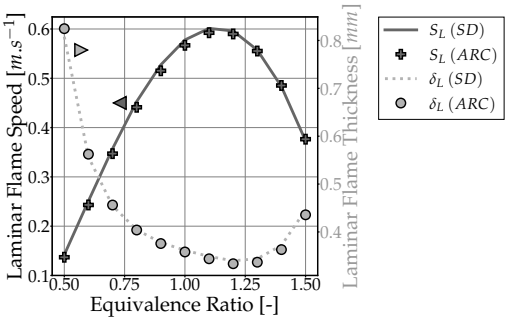

Figure 2: Simulation of a 1D premixed laminar flame using the Analytically Reduced Chemistry computed in [8] at $T = 300\,\mathrm{K}$. Comparison of the laminar flame speed S_L and the thermal flame thickness δ_L.

In the framework of AVBP [11], the convection scheme proposed by Lax and Wendroff [12] is taken along with WALE as a subgrid scale turbulence model [13] (turbulence in the plenum). The CFL and Fourier numbers are set to 0.7 and 0.1 respectively. The computation is stabilized by second and fourth order artificial viscosity terms [14].

To mimic experimental conditions, the channel is initially filled with a mixture at rest corresponding to the stoichiometric condition targeted (experimental equivalence ratios are $\phi = 0.77$, $\phi = 1.03$ and $\phi = 1.19$). The plenum is filled with air. The temperature of the gases is set to $T = 293.0\,\mathrm{K}$. Ignition is forced by imposing a hot temperature sphere at the closed end of the channel over a fixed duration. The sphere temperature profile is Gaussian in time and space, and the maximum temperature is set to $T_{ig} = 3000\,\mathrm{K}$. The ignition sequence lasts 20 ms and is enclosed in a diameter of 2.0 mm. The NSCBC formalism is used for the walls and the outlet [15]. The outlet relaxes to the atmospheric pressure. Wall treatments are the subject of the following section, and can be set to all conditions, from adiabatic to isothermal, passing by heat-loss modeling, with velocity laws.

3 A problem of wall boundary conditions

The first step towards the validation of the simulation setup is the definition of boundary conditions able to properly reproduce the experimental setup. In large explosion cases, the common accepted strategy is to consider that the flame does not have the time to heat up the walls, hence the use of isothermal boundary conditions [16, 17]. A second strategy, often chosen in finger flame theory and simulations is the adiabatic boundary condition [18–20]. In practice, the influence of cold walls on flame acceleration is critical if the flame is reasonably slow: considering adiabatic will tend to promote this acceleration as it suppresses the heat necessarily lost by the flame, and isothermal conditions are only valid under the assumption that the flame is too fast to pre-heat the walls and when thermal resistance is low. It therefore tends to reduce acceleration. Due to the large difference in thermal conductivity between metallic and acrylic surfaces in this experimental scenario, heat fluxes are neither zero (adiabatic), nor the one of the isothermal case, they lie in between and must be modelled. Two approaches are available. The first one consists in coupling fluid simulation to solid simulation in order to resolve unsteady temperature gradients inside the thickness of the walls. The second approach is to consider walls as thermally thin structures and obtain a constant thermal resistance for each surface (strongly linked to the material). In order to obtain preliminary results, the second approach is selected. The first approach is kept for future iterations.

Before elaborating a strategy to determine proper constant thermal resistances, it is necessary to verify that the hypothesis of the thermally thin structure is fulfilled, which is translated by the fact that the conductive heat transfer must dominate the convective one, so that

the heat is transported faster inside the material as by convection at its boundary. The Biot number Bi is introduced to compare convection fluxes to conduction fluxes at the walls and evaluate if the timescales found experimentally validate the hypothesis. $Bi = \frac{h\delta_w}{C_{th}}$ where h is the convective heat transfer coefficient between the fluid and the wall, δ_w is the equivalent wall thickness and C_{th} is the material's thermal conductivity. To estimate h in the present application, the flow at one wall is considered to be burnt gases at $\phi = 1.03$ moving at the average experimental flame front speed $V = 16.8\,\mathrm{m\,s^{-1}}$ over a flat plate. Introducing the Nusselt number Nu, the average of h can be approximated by $Nu\frac{\lambda}{L}$, where $L = 1.0\,\mathrm{m}$ is the length of plate and $\lambda = 0.156\,\mathrm{W\,m^{-1}\,K^{-1}}$ is the thermal conductivity of the burnt gases. As recalled by [21], Nusselt number correlations have been empirically derived, and for a laminar flow parallel to a plane surface it is defined as:

$$Nu \simeq 0.664 Re_L^{\frac{1}{2}} Pr^{\frac{1}{3}} \tag{1}$$

where $Re_L \simeq 6.6 \times 10^{-4}$ is the Reynolds number associated to the length of the tube, and $Pr \simeq 0.68$ is the Prandtl number in the burnt gases ($Re_L < 5.0 \times 10^{-5}$ and $Pr > 0.6$ are in the validity limits). The numerical application gives $h \simeq 17.6\,\mathrm{W\,m^{-2}\,K^{-1}}$. By assuming wall thicknesses of the order of $\delta_w = 2.0\,\mathrm{mm}$, more than an order of magnitude can separate the Biot number at metallic surfaces from the Biot number for optical accesses such that, for example, for stainless steel $C_{th} \simeq 14\,\mathrm{W\,m^{-1}\,K^{-1}}$ gives $Bi_{steel} \simeq 0.0025$ and for acrylic glass $C_{th} \simeq 0.2\,\mathrm{W\,m^{-1}\,K^{-1}}$ gives $Bi_{acrylic} \simeq 0.18$. Two conclusions arise: 1. The low value $Bi_{steel} = 0.0025 \ll 1$ means that metallic surfaces can be considered as thermally thin surfaces, and due to the low thermal resistance of such a material, conditions close to isothermal are reached, 2. The value $Bi_{acrylic} = 0.18 < 0.2$ means that acrylic surfaces are at the limit to be considered as thermally thin under these conditions, and it is important to remain aware that modelling such walls with a constant thermal resistance is partly valid and may introduce errors. Asserting the errors introduced is part of future works where code coupling will be used to solve temperature gradients inside the wall and verify the hypothesis of thin wall made in this preliminary work.

For the approach considered in this paper, constant thermal resistance heat loss $R_{th} = \delta_w / C_{th}$ is chosen. It is proposed to evaluate the effect of this thermal resistance on the flame acceleration by changing the equivalent thickness. Asymptotically, an infinite thickness represents an adiabatic wall, a thickness equals to zero, an isothermal wall. To take into account the difference in materials used for the walls experimentally, it is chosen to model upper and lower channel walls by stainless steel ($C_{th} \simeq 14.0\,\mathrm{W\,m^{-1}\,K^{-1}}$) and the optical access window with acrylic resin ($C_{th} \simeq 0.2\,\mathrm{W\,m^{-1}\,K^{-1}}$). To ensure symmetry, the hanging wall in front of the window is modeled with the same material (See Fig. 3). The same equivalent thickness is used for the four channel walls. The definition of an optimal equivalent wall thickness δ_w^* then follows.

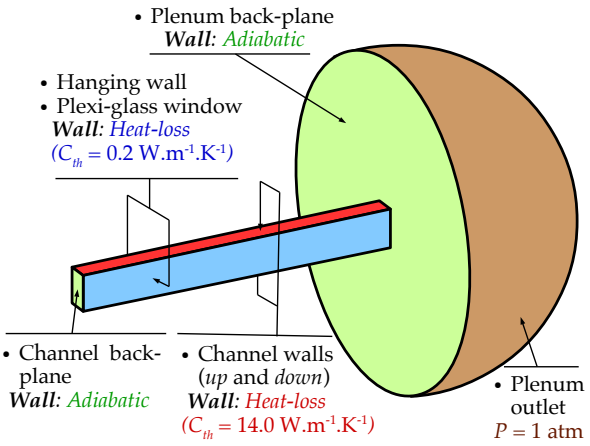

Figure 3: Choice of boundary conditions to experiment the effect of thermal resistance on flame acceleration.

4 A procedure to obtain δ_w^*

The objective of this section is to use a minimal number of simulations to 1. obtain a finer understanding of the influence of heat losses at the walls and 2. propose a fitted equivalent wall thickness that can be further used in various configurations. Four simulations with $\delta_w = 1.0\,\mathrm{mm}$ (close to iso-thermal), $\delta_w = 2.0\,\mathrm{mm}$, $\delta_w = 4.0\,\mathrm{mm}$ and $\delta_w \to +\infty$ (adiabatic) are computed for the case $\phi = 1.03$. To compare cases, a macroscopic measure is proposed under the form of an "error to adiabatic" $\overline{\varepsilon}$, so that for one *case*:

$$\varepsilon(t) = x^{tip}_{adiab}(t) - x^{tip}_{case}(t) \text{ and } \overline{\varepsilon}_N = \frac{1}{N}\sum_{n=0}^{N-1} \varepsilon(n\Delta t) \tag{2}$$

where x^{tip} is the position of the flame tip, Δt is the constant time-step separating two flame tip position evaluations, $[0,\ N\Delta t]$ is the interval on which the average is performed. $N\Delta t$ is chosen to correspond to the onset of the tulip flame in the adiabatic case ($t = 52.0\,\mathrm{ms}$). $\overline{\varepsilon}$ is defined for both simulation cases and experimental cases, such that it is made easy to compare one computational result to the experimental reference and the adiabatic case simulation.

Figure 4 depicts that the error to adiabatic $\overline{\varepsilon}$ decreases with the thickness δ_w, and crosses the error to adiabatic computed for the experimental acquisition. Therefore, there is an optimal thickness δ_w^* to search such that the error to adiabatic of the simulation matches the experiment. However, a very simple question arises: what is a proper fitting procedure to link $\overline{\varepsilon}$ to δ_w^{-1} ? One first initiative could be to produce a linear fit, and correct it successively by adding simulations until convergence is reached. As this is costly, a more convenient approach could be to propose a fitting function that inherits from the physics of the problem, even if a perfect theoretical relation is not obtainable. To start with, let us model the

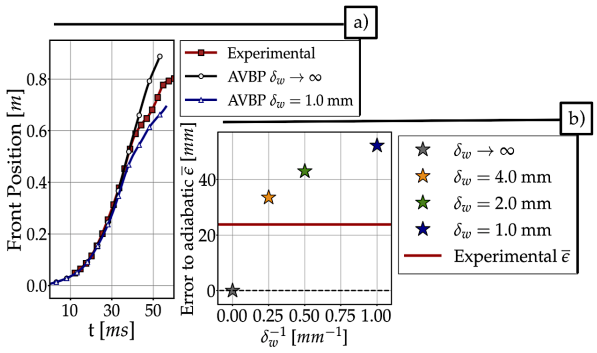

Figure 4: Comparison of flame tip position for varying δ_w: a) Flame front position *versus* time, b) error to adiabatic $\overline{\varepsilon}$.

flame by a finger flame, using the theory of Bychkov *et al.* [19]:

$$\frac{d}{dt}x^{tip} = \frac{\rho_f}{\rho_b}\frac{2}{r_{eq}}Ux^{tip} \tag{3}$$

where ρ_f (resp. ρ_b) is the fresh (resp. burnt) gas density, r_{eq} is the equivalent radius of the flame: $r_{eq} = hw/(h+w)$, with h, w as height and width of the channel. U is the flame propagation speed. In the adiabatic case, $U = U_{adiab}$ (in the theory, $U_{adiab} = S_L$, the laminar flame speed). In order to model the effect of non-adiabatic conditions, a correction is searched to reduce the flame propagation speed so that with losses $U = U_{loss} = U_{adiab} - \alpha$. To find α, the power of the non-adiabatic flame is approximated by:

$$\begin{aligned} c_p(T_b - T_f)\rho_f A U_{loss} = c_p(T_b - T_f)\rho_f A U_{adiab} \\ - (T_b - T_w)\frac{A}{R_{th}} \end{aligned} \tag{4}$$

where c_p is the specific heat, T_f (resp. T_b) is the fresh (resp. burnt) gas temperature, A is the flame surface, T_w is the wall temperature, and R_{th} is the wall thermal resistance. For simplification purposes, $T_w = T_f$, and $R_{th} = \delta_w/C_{th}$. Equation 4 gives:

$$U_{loss} = U_{adiab} - \frac{C_{th}}{\rho_f c_p}\delta_w^{-1} \tag{5}$$

which leads to $\alpha = \frac{C_{th}}{\rho_f c_p}\delta_w^{-1}$. The influence of the equivalent thickness δ_w on flame propagation appears as a corrective term on its propagation velocity. Using the definition of ε given in Eq. 2, an order one differential equation in time is obtained:

$$\frac{d}{dt}\varepsilon = -\frac{2C_{th}}{\rho_b c_p r_{eq}}\delta_w^{-1}\varepsilon \tag{6}$$

With $\sigma = \frac{2C_{th}}{\rho_b c_p r_{eq}}$, and because $\varepsilon(0) = 0$, a constant $B > 0$ exists such that, for $t > 0$, $\varepsilon(t) = B\left(1 - \exp(-\sigma\delta_w^{-1}t)\right)$. Over the interval $[0, N\Delta t]$, the error to adiabatic writes as:

$$\overline{\varepsilon}_N = B\left(1 - \frac{1}{N}\frac{1-\exp(-\sigma\Delta t\,\delta_w^{-1}N)}{1-\exp(-\sigma\Delta t\,\delta_w^{-1})}\right) \tag{7}$$

Asymptotically, the relation is coherent with the fact that when going closer to adiabatic, δ_w tends towards infinity, the ratio containing the exponential terms is equivalent to N/N, thus leading to $\lim_{\delta_w \to +\infty}\overline{\varepsilon}_N = 0$. Similarly, when reaching isothermal boundary, δ_w tends towards 0, leading to $\lim_{\delta_w \to 0}\overline{\varepsilon}_N = B(1-1/N)$, a positive constant depending on the width of the averaging interval. It is important to notice that the relation obtained in Eq. 7 is only valid for a very restrained area (early finger flame, before the flame touches the wall) and *a priori*, it does not apply to the problem at hand. Therefore, it is not necessary to try to search directly numerical values of B and σ. However, it gives information on the type of function that could lead to a proper fitting of $\overline{\varepsilon}$ as a function of δ_w^{-1}. It guides towards searching a function under the form:

$$f_{fit}(\delta_w^{-1}, N) = B'\left(1 - \frac{1}{N}\frac{1-\exp(-\sigma'\delta_w^{-1}N)}{1-\exp(-\sigma'\delta_w^{-1})}\right) \tag{8}$$

where B' and σ' are the parameters to fit. Under this assumption, a simple fitting procedure can be performed on the results depicted in Fig. 4 which leads to the constants $B' = 60.24$ mm and $\sigma' = 0.19$ mm, for $N = 40$ steps. The model is shown in Fig. 5. Thanks to this simple fit, it is possible to obtain the optimal δ_w^* which corresponds to an equivalent thickness of 6.73 mm. A simulation is performed with this value and added to Fig. 5. A relative error in $\overline{\varepsilon}$ inferior to 15 % is reached for this fifth computation (4 simulations are run to prepare the value of δ_w^*, a fifth to confirm the value). At this step, there are two possibilities: 1. this error is evaluated to be sufficiently low, and the value of δ_w^* is kept to continue the study, or 2. the model is fitted using the current value of δ_w^* and a new optimal is found (see Fig. 5: the model fitted *a posteriori*), a new simulation closer to the experimental $\overline{\varepsilon}$ could be obtained.

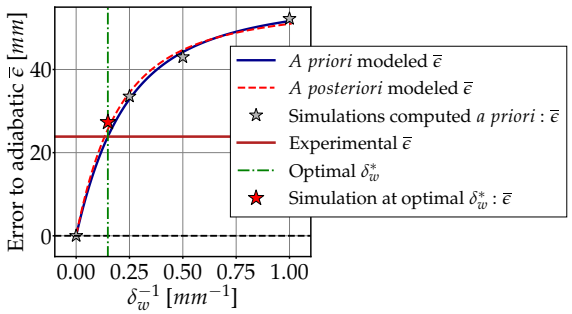

Figure 5: Model of the error to adiabatic as a function of δ_w^{-1}, simulation results *a priori* and *a posteriori*.

To remain coherent with the fact that the objective of this fitting procedure was to help finding rapidly an optimum with a minimal number of simulations obtained *a priori*, it is decided to continue with the already computed δ_w^*. In the next sections, and with this value of δ_w^*, a complete validation of the simulation setup *versus* experimental results can be done, including comparisons to cases with different equivalence ratios.

5 Complete experimental/simulation validation

For this validation, three equivalence ratios are asserted: $\phi = 1.03$, $\phi = 1.19$, and $\phi = 0.77$ using δ_w^*. For the three cases, tulip flames form and propagate (see Fig. 6). Figure 7 compares flame front position and velocity for simulation and experimental cases. Concerning flame tip position, a good agreement is reached for the three equivalence ratios targeted. To measure the drift of the simulation in comparison to the experiment, the average error with respect to the experimental results $\overline{\varepsilon}_{exp}$ is computed:

$$\overline{\varepsilon}_{exp} = \frac{1}{N}\sum_{n=0}^{N-1}\left(x_{sim}^{tip}(n\Delta t) - x_{exp}^{tip}(n\Delta t)\right) \qquad (9)$$

where $[0, N\Delta t]$ is the interval where experimental results exist. For $\phi = 1.03$ (resp. $\phi = 1.19$ and $\phi = 0.77$), this average drift reaches +2.7 mm (resp. −16.8 mm and +26.2 mm). The low absolute value for $\phi = 1.03$ is reassuring as it confirms that the fitting procedure allows to successfully capture the flame displacement. For $\phi = 1.19$ the negative value means that, on average, the simulated flame lags behind the experimental flame, but this lag remains low for a flame propagating in a 1.0 m-long tube, and an explosion event that lasts more than 70.0 ms. The conclusion is similar for $\phi = 0.77$, where the positive drift is of the order of magnitude of the hundredth of the tube length. In addition, the relative error on the peak velocity $\left|V_{sim}^{peak} - V_{ref}^{peak}\right| / V_{ref}^{peak}$ is computed, and reaches 5.3 % at $\phi = 1.03$, 10.9 % at $\phi = 1.19$, and 4.1 % at $\phi = 0.77$. Additionally, the transition position defined as the flame front position at which the simulated peak velocity is reached is 83.9 mm behind experimental at $\phi = 1.03$, 101.9 mm behind at $\phi = 1.19$, and 23.6 mm behind at $\phi = 0.77$ which represents errors of the order of 10 % of the tube length. Thus, finger-tulip transition position is only reasonably well predicted by simulation for the three equivalence ratios considered, and it remains a subject of improvement for future works.

The comparison of overpressure sensor data to computed overpressure gives further information on the quality of the simulation. Maximum overpressure levels for the first sensor (PT1) are well retrieved by simulation (with relative errors lower than 10 % for all the equivalence ratios). The temporal succession of pressure peaks is predicted consistently, with two positive impulses followed by a negative one. However, the negative peak that follows is underpredicted by simulation. Finally, the effect of large oscillations assumed to be due to acoustic resonance of the tube are not perfectly recovered by simulation. To sum up concerning pressure measurements, global levels and temporal responses are satisfactorily predicted. Differences are observed, and there are multiple ways to try and reduce them such as computing the acoustics at a laboratory scale to see its influence on tube resonance or improving the mesh refinement inside the channel.

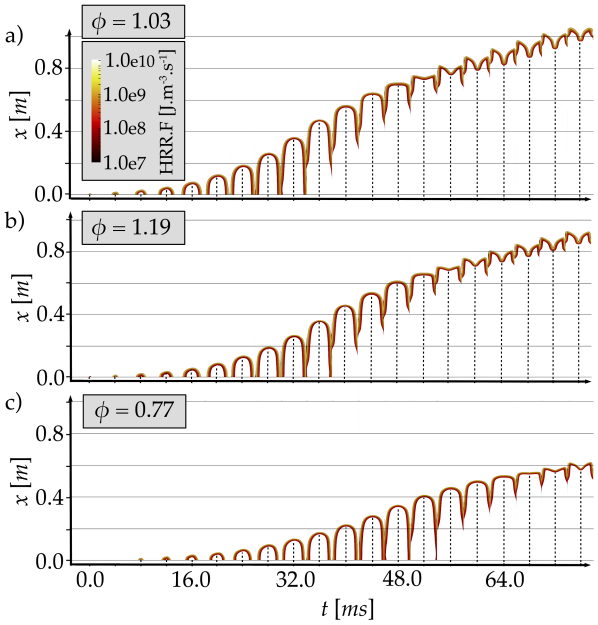

Figure 6: Flame propagation depicted as a z-normal cut of the heat release rate multiplied by thickening, with the optimal δ_w^*: a) at $\phi = 1.03$ b) at $\phi = 1.19$, c) at $\phi = 0.77$.

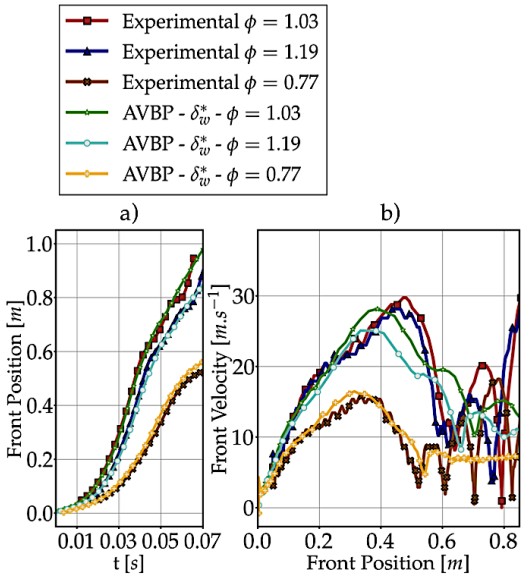

Figure 7: Experimental/simulation comparison of flame tip position and velocity for δ_w^*: a) Flame front position *versus* time, b) Flame front velocity *versus* the flame front position.

Conclusion

Through experimental *versus* simulation comparisons of flame front position/velocity and overpressure measurements, it is possible to validate the use of the simulation setup proposed here for the reproduction of finger-to-tulip flame transitions inside a rectangular channel with Li-ion vent gases at three different equivalence ratios. The effect of wall heat losses is observed, and a simple fitting procedure helps to close the gap between experimental and simulation by computing an optimal equivalent wall thickness δ_w^*. Thanks to this famil-

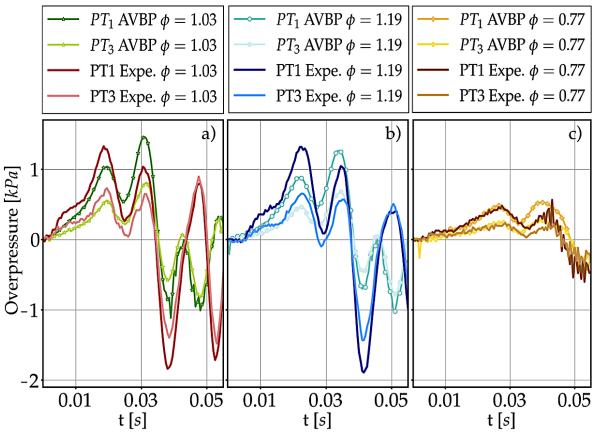

Figure 8: Experimental/simulation comparison of PT1 and PT3 sensors overpressure for δ_w^*: a) at $\phi = 1.03$, b) at $\phi = 1.19$, c) at $\phi = 0.77$.

iarization with the problem of explosion of Li-ion vent gases, it is possible to continue with the test of configurations where turbulence interacts with the flame [22]. Knowing that the history effect can be crucial in explosions, the proper capture of the initial laminar phase improves the confidence in the feasibility of high fidelity simulations of realistic cases.

Acknowledgements

This work received support from SAFT batteries *(111 Bd. Alfred Daney, 33074 Bordeaux, France)* and TotalEnergies *(OneTech, 92400 Courbevoie, France)*. It was performed using HPC resources from GENCI-IDRIS (Grant 2022 - A0112B10157).

References

[1] A. R. Baird, E. J. Archibald, K. C. Marr, and O. A. Ezekoye, Explosion hazards from lithium-ion battery vent gas, *J. Power Sources* **446** (2020).

[2] Q. Wang, P. Ping, X. Zhao, G. Chu, J. Sun, and C. Chen, Thermal runaway caused fire and explosion of lithium ion battery, *J. Power Sources* **208** (2012).

[3] F. Larsson, P. Andersson, and B. E. Mellander, Lithium-ion battery aspects on fires in electrified vehicles on the basis of experimental abuse tests, *Batteries* **2** (2016).

[4] F. Larsson, J. Anderson, P. Andersson, and B.-E. Mellander, Thermal Modelling of Cell-to-Cell Fire Propagation and Cascading Thermal Runaway Failure Effects for Lithium-Ion Battery Cells and Modules Using Fire Walls, *Journal of The Electrochemical Society* **163** (2016).

[5] S. Gao, L. Lu, M. Ouyang, Y. Duan, X. Zhu, C. Xu, B. Ng, N. Kamyab, R. E. White, and P. T. Coman, Experimental Study on Module-to-Module Thermal Runaway-Propagation in a Battery Pack, *J. Electrochem. Soc.* **166** (2019).

[6] M. Henriksen, K. Vaagsaether, J. Lundberg, S. Forseth, and D. Bjerketvedt, Simulation of a premixed explosion of gas vented during Li-ion battery failure, *Fire Safety J.* **126** (2021).

[7] FAA, Tech. Rep. (2016).

[8] A. Cellier, F. Duchaine, T. Poinsot, G. Okyay, M. Leyko, and M. Pallud, An analytically reduced chemistry scheme for large eddy simulation of lithium-ion battery fires, *Combust. Flame* **In Press** (2023).

[9] J. P. Legier, T. Poinsot, and D. Veynante, in *Proceedings of the Summer Program, Centre for Turbulence Research* (2000).

[10] T. Jaravel, Ph.D. thesis (2016).

[11] Cerfacs, AVBP CFD solver, https://www.cerfacs.fr/avbp7x/.

[12] P. Lax and B. Wendroff, Tech. Rep. (1959).

[13] F. Nicoud and F. Ducros, Subgrid-scale stress modelling based on the square of the velocity, *Flow Meas. Instrum.* **62** (1999).

[14] A. Jameson, W. Schmidt, and E. Turkel, Numerical solution of the Euler equations by finite volume methods using Runge Kutta time stepping schemes, *AIAA Fluid and Plasma Dyn. Conf.* (1981).

[15] T. J. Poinsot and S. K. Lele, Boundary conditions for direct simulations of compressible viscous flows, *J. Comput. Phys.* **101** (1992).

[16] P. Quillatre, O. Vermorel, T. Poinsot, and P. Ricoux, Large eddy simulation of vented deflagration, *Ind. Eng. Chem. Res.* **52** (2013).

[17] O. Vermorel, P. Quillatre, and T. Poinsot, LES of explosions in venting chamber: A test case for premixed turbulent combustion models, *Combust. Flame* **183** (2017).

[18] V. Akkerman, V. Bychkov, A. Petchenko, and L. E. Eriksson, Accelerating flames in cylindrical tubes with nonslip at the walls, *Combust. Flame* **145** (2006).

[19] V. Bychkov, V. Akkerman, G. Fru, A. Petchenko, and L. E. Eriksson, Flame acceleration in the early stages of burning in tubes, *Combust. Flame* **150** (2007).

[20] V. Bychkov, V. Akkerman, D. Valiev, and C. K. Law, Influence of gas compression on flame acceleration in channels with obstacles, *Combust. Flame* **157** (2010).

[21] G. Maragkos and T. Beji, Review of convective heat transfer modelling in cfd simulations of fire-driven flows, *Appl. Sci.* **11** (2021).

[22] M. Henriksen, K. Vaagsaether, J. Lundberg, S. Forseth, and D. Bjerketvedt, Numerical study of premixed gas explosion in a 1-m channel partly filled with 18650 cell-like cylinders with experiments, *J. Loss Prevent. Proc. Ind.* **77** (2022).